

# Study of Magnetic and Dielectric Behaviour of Ni doped Fe<sub>2</sub>O<sub>3</sub> Nanopowders

\*M. Imran<sup>1)</sup>, Saira Riaz<sup>2)</sup>, Zohra N. Kayani<sup>3)</sup> and Shahzad Naseem<sup>4)</sup>

<sup>1), 2), 4)</sup> *Centre of Excellence in Solid State Physics, University of Punjab, Lahore, Pakistan*

<sup>3)</sup> *Department of Physics, LCWU, Lahore, Pakistan*

<sup>2)</sup> [saira.cssp@pu.edu.pk](mailto:saira.cssp@pu.edu.pk)

## ABSTRACT

Nano-sized magnetic nanoparticles (NPs) are of particular interest in various technological applications. Iron oxide nanoparticles exhibit distinctive properties due to their reduced size. In order to explore these properties, undoped and nickel doped iron oxide NPs are prepared using sol-gel method. Dopant concentration is varied as 0 – 10%. XRD results confirm the formation of Fe<sub>2</sub>O<sub>3</sub> phase of iron oxide. Crystallinity of NPs increases as dopant concentration is increased to 8%. SEM results show reduction in grain size with increase in dopant concentration up to 8%. Magnetic properties show transition from weak ferromagnetic to strong ferromagnetic behavior up to a Ni content of 8%. Ferromagnetic behavior in Fe<sub>2</sub>O<sub>3</sub> NPs is associated with exchange interaction between spins of electrons that are trapped in oxygen vacancies and increases as Ni<sup>2+</sup> replaces Fe<sup>3+</sup> cations in the host lattice. Dielectric constant shows sharp increase as dopant concentration is increased to 8%. Further increase in dopant concentration results in decreased dielectric constant and increase in tangent loss.

## 1. INTRODUCTION

Iron oxide is extensively found in nature. Whenever iron metal is exposed to air, it reacts with oxygen present in the atmosphere, and becomes iron oxide. So, we can say that iron oxide is present around us so long as iron metal and oxygen are present on the planet earth. It has been immensely and successfully used in various fields of life by humans. It has been chiefly used in various technological applications and is also being used in many biological and geological fields. In early days Iron oxides were particularly used as pigments and dyes. In this era applications of iron oxide have been spreading in various fields including gas sensors, photo electrochemistry, and magnetic storage devices, for cancer treatment and also in electrochromism (Meng et al. 2016, Riaz et al. 2013, Jiang et al. 2011).

Uses of iron oxides in different fields strongly depend on different phases of iron

oxide. These different phases of iron oxide depend on stoichiometry, crystallographic system, type of structure and chemical state. Two states of oxidation are present in iron oxide which are  $\text{Fe}^{2+}$  (ferrous) and  $\text{Fe}^{3+}$  (ferric) (Riaz et al. 2014a-c, Akbar et al. 2014a).

Among different phases of iron oxide, hematite ( $\alpha\text{-Fe}_2\text{O}_3$ ) offers its applications in magnetic, optical and spintronic devices.  $\alpha\text{-Fe}_2\text{O}_3$  is abundant in nature and has a band gap of 2.2eV (Riaz et al. 2014a, Akbar et al. 2014a, Glasscock et al. 2008). The hexagonal unit cell of hematite consists of six formula units. The lattice parameters are  $a=5.03\text{\AA}$  and  $c=13.75\text{\AA}$ . Another convention to describe the unit cell of hematite is in rhombohedral crystal system. In this case the lattice parameters are  $a=5.43\text{\AA}$  and  $\alpha=55^\circ$ . Spin orbit interaction between the planes of hematite leads to magnetization. This magnetization arises due to uncompensated magnetic moments of  $\text{Fe}^{3+}$  cations. This magnetic moment of hematite can be further enhanced/improved with doping strategies. These doping strategies are based on ionic radius and valence state difference in host and dopant ions (Riaz et al. 2014a, Akbar et al. 2014a, Aragon et al. 2016).

For this purpose, nickel doped iron oxide nanoparticles are prepared with dopant concentration 2%, 4%, 6% and 8%. Correlation between magnetic and dielectric properties is investigated in detail.

## 2. EXPERIMENTAL DETAILS

Synthesis of pure hematite phase was carried out using inexpensive and low temperature sol-gel method. Sol synthesis was carried out by using iron nitrate, nickel nitrate, water and ethylene glycol. Detailed sol-gel procedure was reported earlier (Riaz et al. 2014a). Iron oxide sols were spin coated on copper substrate (1cm x 1cm). Structural characterization is reported by using Bruker D8 Advance X-ray Diffractometer with  $\text{Cu K}\alpha$  radiations ( $\lambda=1.5406\text{\AA}$ ). Lakeshore's 7407 Vibrating Sample Magnetometer was used for studying the magnetic properties. Wein Kerr 6500B Impedance analyzer is used for the dielectric characterization of Nickel Doped  $\text{Fe}_2\text{O}_3$  Nanopowders.

## 3. RESULTS AND DISCUSSION

XRD patterns for iron oxide thin films can be seen in Fig. 1. The peaks are indexed according to JCPDS card no. 87-1165. All the peaks are matched with hematite phase of iron oxide ( $\alpha\text{-Fe}_2\text{O}_3$ ). No extra peaks associated with nickel oxide or other phases of iron oxide were observed for entire concentration range studied. However, diffraction peaks corresponding to planes (104) and (113) shifted to slightly higher angles thus resulting in contraction in volume of unit cell. This is because of the difference in ionic radii of nickel and iron.

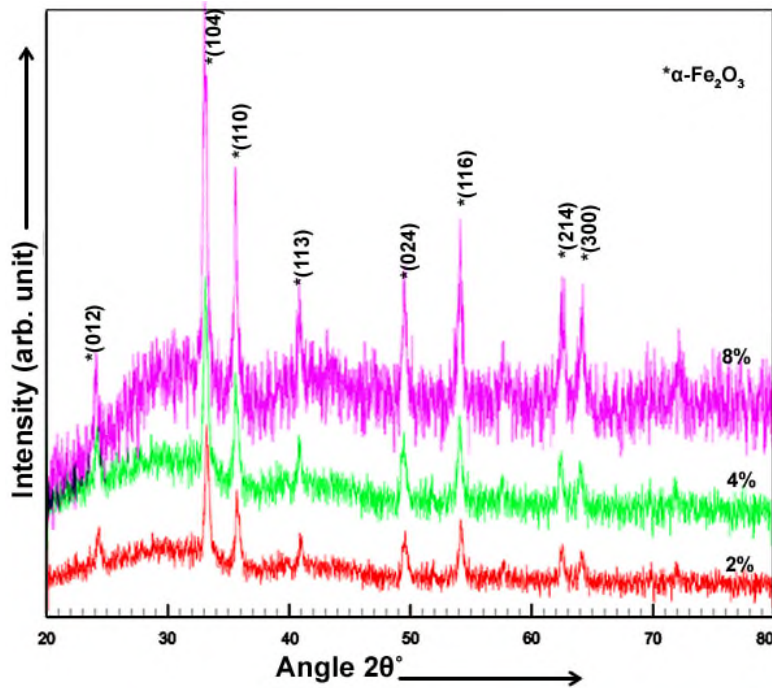


Fig. 1 XRD patterns for Ni doped Fe<sub>2</sub>O<sub>3</sub> nanopowders (\*α-Fe<sub>2</sub>O<sub>3</sub>)

Table 1 Lattice parameters and unit cell volume for Ni doped α-Fe<sub>2</sub>O<sub>3</sub>

Dopant concentration (%)	Lattice parameters (Å)		Unit cell volume (Å <sup>3</sup> )
	a	c	
2	5.021	13.70	299.1017
4	5.018	13.698	298.7008
6	5.012	13.623	296.3554
8	5.008	13.601	295.4047

Crystallite size (Cullity 1956) and dislocation density (Kumar et al. 2011) were calculated using Eqs. 1-2 respectively

$$t = \frac{0.9\lambda}{B \cos \theta} \quad (1)$$

$$\delta = \frac{1}{t^2} \quad (2)$$

Where,  $\theta$  is the diffraction angle,  $\lambda$  is the wavelength (1.5406Å) and  $B$  is Full Width at Half Maximum. Crystallite size increases as Ni concentration increases from 2% to 8%. This Increase implies that dopant atoms are properly incorporated in the host lattice. As a result of which, dislocation density is reduced in nanopowders. Changes in lattice parameters and crystallite size indicate that Ni has effectively replaced Fe sites in α-Fe<sub>2</sub>O<sub>3</sub>.

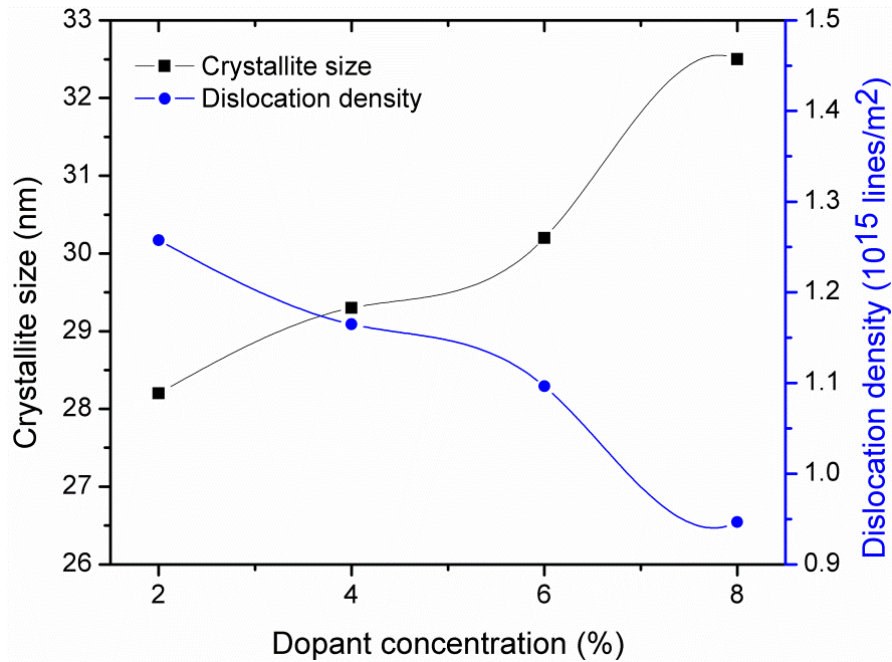


Fig. 2 Crystallite size and dislocation density plotted as a function of dopant concentration

Magnetic hysteresis loops for Ni doped  $\alpha$ - $\text{Fe}_2\text{O}_3$  nanopowders can be seen in Fig. 3. These nanopowders at dopant concentration 2-6% show weak magnetic behavior. In  $\alpha$ - $\text{Fe}_2\text{O}_3$  structure two sublattices are present. The spins in the two different sublattices have antiparallel arrangement. Spins in the same lattice have parallel arrangement. Because of spin orbit coupling  $\text{Fe}^{3+}$  cations have some uncompensated spins. These uncompensated spins induce weak magnetic behavior in  $\alpha$ - $\text{Fe}_2\text{O}_3$ . This weak magnetic behavior transforms to strong ferromagnetic behavior at dopant concentration 8%. This ferromagnetic behavior in  $\alpha$ - $\text{Fe}_2\text{O}_3$  NPs is associated with exchange interaction between spins of electrons that are trapped in oxygen vacancies and increase as  $\text{Ni}^{2+}$  replaces  $\text{Fe}^{3+}$  cations in the host lattice (Craik 1975).

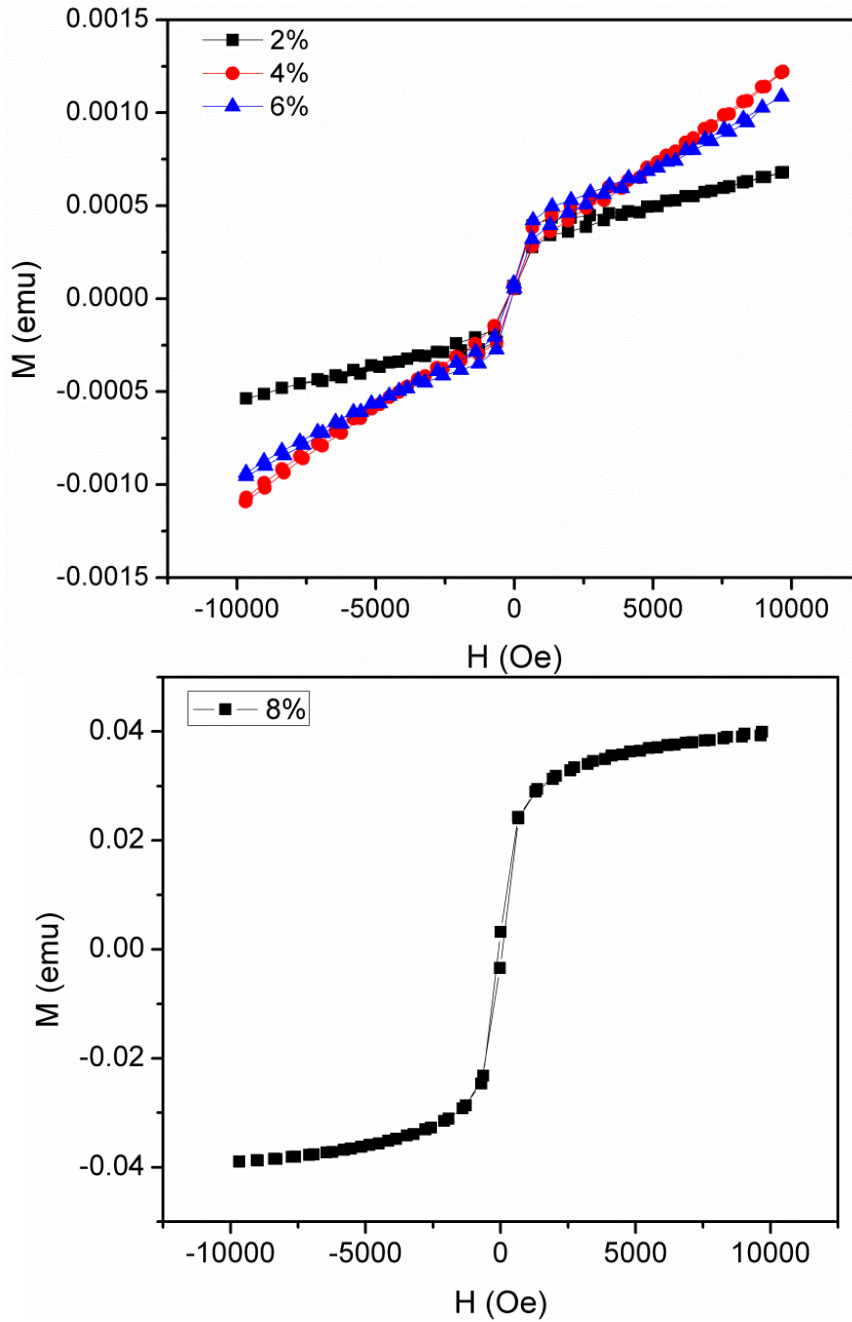


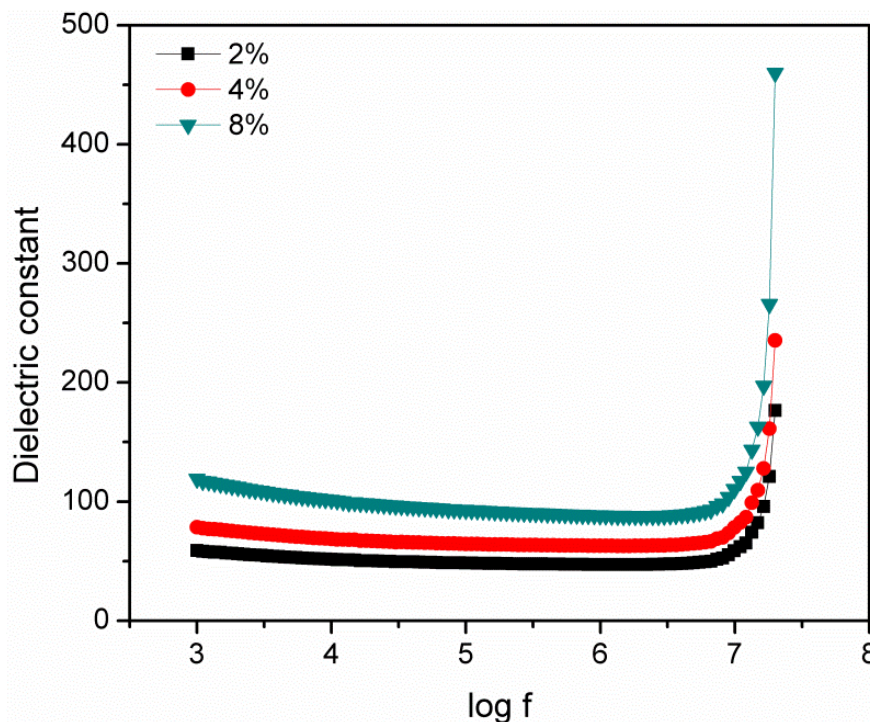
Fig. 3 M-H curves for Ni doped Fe<sub>2</sub>O<sub>3</sub> nanopowders

Dielectric constant ( $\epsilon$ ) and tangent loss ( $\tan \delta$ ) were determined using Eqs. 3 and 4 (Barsoukov and Macdonald 2005)

$$\epsilon = \frac{Cd}{\epsilon_0 A} \quad (3)$$

$$\tan \delta = \frac{1}{2\pi f \epsilon_0 \epsilon \rho} \quad (4)$$

Where,  $C$  is the capacitance,  $\epsilon_0$  is the permittivity of free space,  $A$  is the area,  $f$  is the frequency and  $\rho$  is the resistivity. Both dielectric constant and tangent loss show decreasing trend at lower frequencies. This decrease arises due to space charge carriers in a dielectric material. These charge carriers can only follow the field alteration at low frequencies. (Riaz et al. 2015, Jamal et al. 2011). This behavior is also depicted by Maxwell Wagner Model. The electrons travel through grains and reach grain boundaries. This leads to space charge polarization. Furthermore, space charge polarization, electron displacement polarization and turning direction polarization all only contribute at low frequencies. While only electron displacement polarization contributes at high frequencies. This results in initial decrease in dielectric constant and tangent loss (Jamal et al. 2008). The increase in dielectric constant at high frequencies is attributed to resonance effect. Resonance occurs when jumping frequency of ions becomes equal to field frequency (Jamal et al. 2008). It can be seen that dielectric constant increases from 45 to 75 and 98 ( $\log f = 5.0$ ) (Fig. 5) as dopant concentration was increased from 2% to 4% and 8%, respectively. This increase in dielectric constant is associated with increase in crystallite size as dopant concentration was increased and associated decrease in dislocation density (Fig. 2). This leads to increase in probability of the formation of  $180^\circ$  domains that offers high polarization capabilities. This results in increase in dielectric constant and decrease in tangent loss.



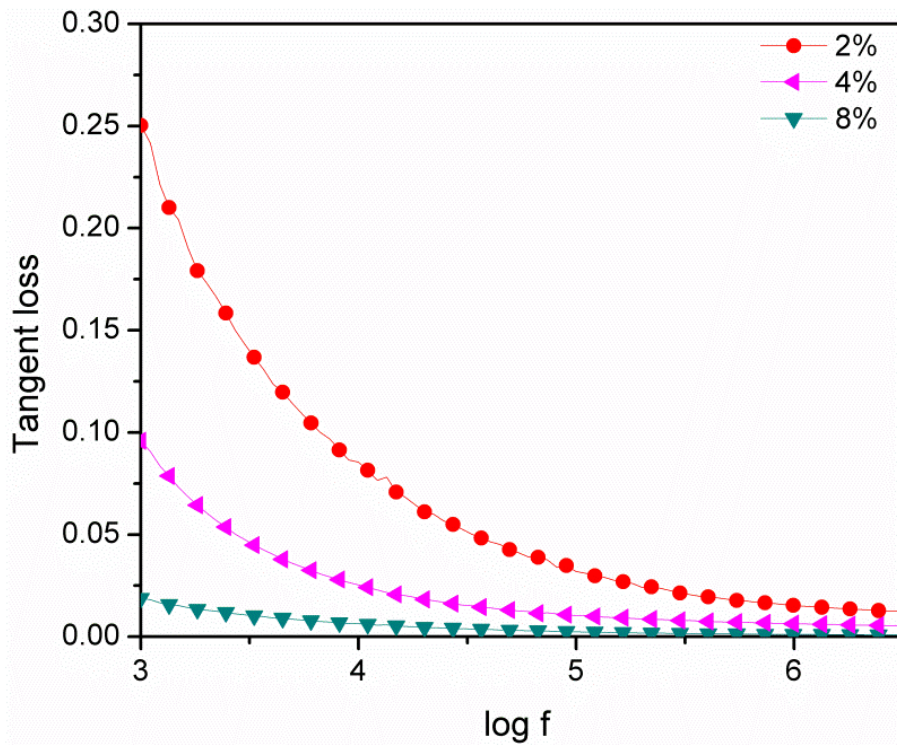


Fig. 4 Dielectric constant and tangent loss for Ni doped Fe<sub>2</sub>O<sub>3</sub> nanopowders

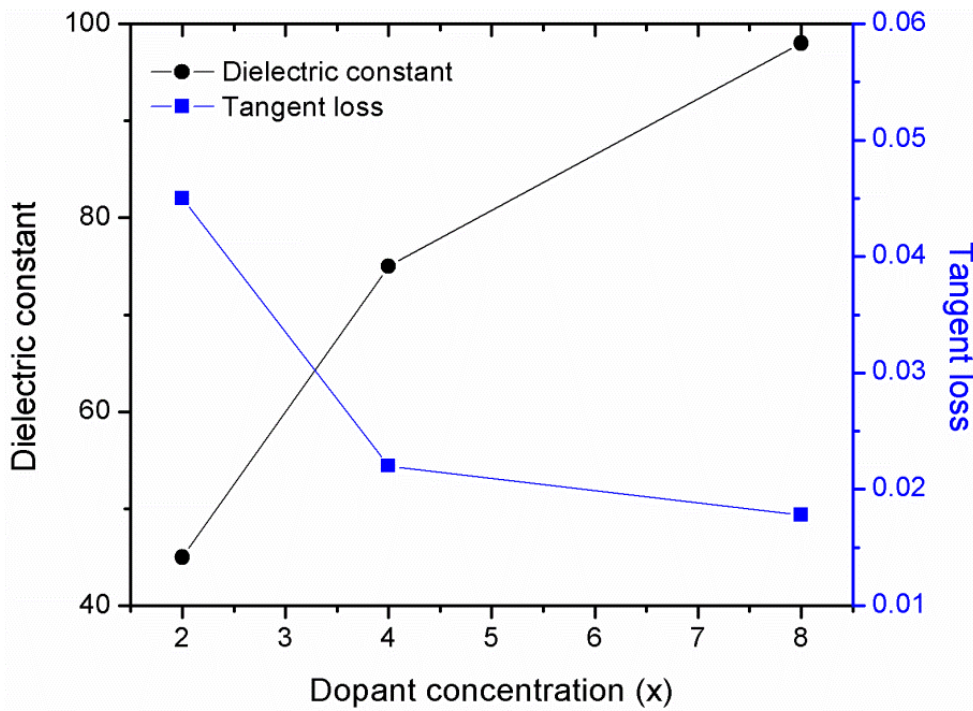


Fig. 5 Dielectric constant and tangent loss for Ni doped Fe<sub>2</sub>O<sub>3</sub> nanopowders

## 4. CONCLUSIONS

Ni doped  $\alpha$ -Fe<sub>2</sub>O<sub>3</sub> nanoparticles were synthesized through sol-gel route. Dopant concentration was varied as 2%-8%. Formation of  $\alpha$ -Fe<sub>2</sub>O<sub>3</sub> phase was confirmed using XRD. Dielectric constant showed anomalous behavior while normal dispersion was observed in tangent loss. Increase in dielectric constant was observed with increase in dopant concentration upto 8%. Magnetic properties showed transition from weak magnetic to strong ferromagnetic behavior at 8% Ni concentration.

## REFERENCES

- Akbar, A., Riaz, S., Ashraf, R. and Naseem, S. (2014(b)), "Magnetic and magnetization properties of Co-doped Fe<sub>2</sub>O<sub>3</sub> thin films," *IEEE Trans. Magn.*, **50**, 2201204
- Akbar, A., Riaz, S., Ashraf, R. and Naseem, S. (2014a), "Magnetic and magnetization properties of Co-doped Fe<sub>2</sub>O<sub>3</sub> thin films," *IEEE Trans. Magn.*, **50**, 2201204
- Akbar, A., Riaz, S., Bashir, M. and Naseem, S. (2014a), "Effect of Fe<sup>3+</sup>/Fe<sup>2+</sup> Ratio on Superparamagnetic Behavior of Spin Coated Iron Oxide Thin Films," *IEE Trans. Magn.*, **50**, 2200804.
- Aragon, F.F.H., Ardisson, J.D., Aquinoa, J.C.R., Gonzalez, I., Macedo, W.A.A., Coaquira, J.A.H., Mantilla, J., Silva, S.W. and Morais, P.C. (2016), "Effect of the thickness reduction on the structural, surface and magnetic properties of  $\alpha$ -Fe<sub>2</sub>O<sub>3</sub> thin films," *Thin Solid Films*, **607**, 50–54.
- Cullity, B.D. (1956), "Elements of x-ray diffraction," Addison Wesley Publishing Company, USA.
- Glasscock, J.A., Barnes, P.R.F., Plumb, I.C., Bendavid, A. and Martin, P.J. (2008), "Structural, optical and electrical properties of undoped polycrystalline hematite thin films produced using filtered arc deposition," *Thin Solid Films*, **516**, 1716–1724.
- Jamal, E.M.A., Kumar, D.S. and Anantharaman, M.R. (2011), "On structural, optical and dielectric properties of zinc aluminate nanoparticles," *Bull. Mater. Sci.*, **34**, 251–259.
- Jiang, K.L., Lai, H., Hu, X.B., Zeng, F., Lan, K.X., Liu, Y., Wu, Z. W. and Gu, J. (2011), "The effect of [Fe<sup>3+</sup>]/[Fe<sup>2+</sup>] molar ratio and iron salts concentration on the properties of superparamagnetic iron oxide nanoparticles in the water/ethanol/toluene system", *Nanopart. Res.*, **13**, 5135.
- Kumar, N., Sharma, V., Parihar, U., Sachdeva, R., Padha, N. and Panchal, C.J. (2011) "Structure, optical and electrical characterization of tin selenide thin films deposited at room temperature using thermal evaporation method," *J. Nano- Electron. Phys.*, **3**, 117-126
- Meng, Q., Wang, Z., Chai, X., Weng, Z., Ding and R., Dong, L. (2016), "Fabrication of hematite ( $\alpha$ -Fe<sub>2</sub>O<sub>3</sub>) nanoparticles using electrodeposition," *Appl. Surf. Sci.*, **368**, 303-308.
- Riaz, S., Akbar, A. and Naseem, S. (2013), "Structural, electrical and magnetic properties of iron oxide thin films," *Adv. Sci. Lett.*, **19**, 828-833.



- Riaz, S., Akbar, A. and Naseem, S. (2014a), "Ferromagnetic Effects in Cr-Doped Fe<sub>2</sub>O<sub>3</sub> Thin Films," *IEEE Trans. Magn.*, **50**, 2200704
- Riaz, S., Ashraf, R., Akbar, A. and Naseem, S. (2014b), "Free Growth of Iron Oxide Nanostructures by Sol-Gel Spin Coating Technique—Structural and Magnetic Properties," *IEE Trans. Magn.*, **50**, 2301805.
- Riaz, S., Shah, S.M.H., Akbar, A., Atiq, S., Naseem, S. (2015), "Effect of Mn doping on structural, dielectric and magnetic properties of BiFeO<sub>3</sub> thin films," *J. Sol-Gel Sci. Technol.*, **74**, 329-339